Frequency Selective Surfaces using Sinuous elements 3D-printed

Pedro Vazquez Rodriguez(1), Cesar Briso(1)
pedro.vazquezr@alumnos.upm.es, cesar.briso@upm.es
(1) Dept. IAC. Technical University of Madrid, ETSI Sistemas Telecomunicacion, c/Nikola Tesla sn, 28031 Madrid, Spain

***Abstract*- A flat periodic FSS (frequency –selective surface) is presented fully manufactured with a standard 3D printer and commercial dielectric and conductive PLA filament. The absorber is comprised of graphite filled polylactic acid (PLA) two-dimensional array of sinuous elements, backed by a PLA substrate and graphite filled PLA ground plane. The absorber was optimized for 8 to 12 GHz and offers a 10 dB reflection reduction bandwidth BW of 52.38% (7.44-12.72 GHz) for both polarizations. The thickness of the proposed absorber is less than 0.125 λ_L (wavelength at the lowest cutoff frequency f_L). The results provided shown the possibilities of this printing technology,**

I. INTRODUCTION

Frequency selective surface (FSS) can be used as a spatial filter that allow the reflection or absorption of a specific frequency band [1], [2]. These structures can be used to reflect signals with low power loss, while out-of-band waves are absorbed and strongly attenuated. Most of the applications of electromagnetic FSS are radome design to protect antennas [3] or to reduce the radar signature of a system at a specific frequency range [4] improving the performance of classical absorbers.

FSS can be implemented replacing the homogeneous resistive surface traditionally used by a surface covered with lossy periodic frequency resonant elements . These types of absorbers usually have wide bandwidth and can be designed as low pass, band stop of high pass . These structures can be built of two types: multilayer planar structures conformed onto a three-dimensional profile [5] or 3D structures [6].

This paper presents the results of an investigation on the design of a band stop frequency selective multilayer planar absorber operating from 2 to 18 GHz with a stop band from 7 to 13Ghz . The structure is based on the use of an array of sinuous elements built on a 3D multilayer structure. The structure is 5mm thick (0.125 λ_L) and has been built using a 3D printer and conductive [7] and standard dielectric PLA filament.

II. DESIGN OF THE ABSORBER

A. Modeling of the Absorber

The absorber is made up of three layers manufactured solely by fused deposition modeling (FDM) 3D printing. The topmost layer of the absorber is comprised of a carbon filled PLA sinuous element as described in B. The dielectric backing is manufactured using a t_S thick structure of PLA with a 25% infill, overall dielectric constant ϵ_r of 1.44 and overall loss tangent $\tan\delta$ of 0.003 [8], [9]. The ground plane is made up by a solid layer of carbon filled PLA with a thickness of t_{CG}. The periodic unit cell structure is spaced D over the two-dimensional array. The layout can be observed in Fig. 1 1.

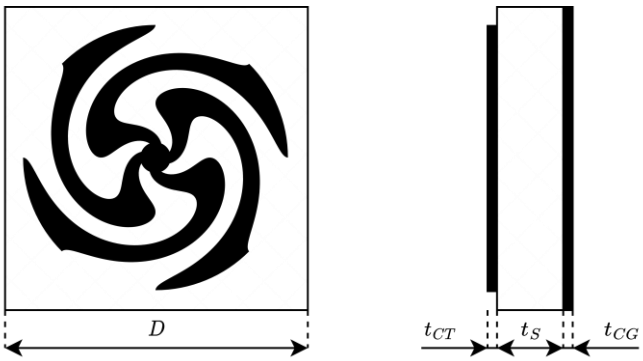

Fig. 1. Layout of the unitary cell.

B. The Sinuous Element

The FSS of this absorber is made up of a sinuous element connected internally by a solid circle with a radius r_{in}. First introduced in 1987, DuHamel publishes a patent for the design of the sinuous antenna, which combines properties from the frequency-independent spiral antennas and log-periodic antennas [10]. The design provides ultra-wideband (UWB) radiation with polarization diversity in a form factor similar to a spiral design [10]. In order to alleviate the fabrication tolerances, the sinuous curve proposed follows a modified linear expansion [11]. To mitigate the unwanted resonance, a trimming technique such as the one demonstrated by Crocker is employed [12]. Equation (1) describes the modified linear expanding sinuous curve without Croker's trim.

$$\begin{cases} x(t)=t\cdot\cos\left(\sin\left(2\pi\cdot N\cdot\frac{t-r_{in}}{r_{out}-r_{in}}\right)\cdot(\alpha-\delta)\pm\delta\right) \\ y(t)=t\cdot\sin\left(\sin\left(2\pi\cdot N\cdot\frac{t-r_{in}}{r_{out}-r_{in}}\right)\cdot(\alpha-\delta)\pm\delta\right) \end{cases} \quad t\in[r_{in},r_{out}] \tag{1}$$

Where r_{in} indicates the curve inner radius, r_{out} indicates the curve outer radius, N indicates number of full 2π periods in the curve, α indicates the maximum amplitude of the curve sine, δ indicates the offset between the two edges of the curve. To apply the trim, a circle or radius r_{trim} intersects the sinuous curve. Equation (2) calculates r_{out} as a function of r_{trim}.

$$r_{out} = -\frac{r_{trim}\cdot N - 0.25\cdot r_{in}}{N\cdot\left(-1+\frac{0.25}{N}\right)} \quad (2)$$

The complete sinuous element is displayed in Fig. 11.

C. Characterization of the Conductive PLA.

One of the key elements of the design is the modeling of the conductive PLA used for the manufacturing of top and bottom layers. Several graphite filled PLA has been tested but the best balance between printing quality and resistivity has been obtained using graphite filled PLA manufactured by Capifil. This filament offers a DC surface resistivity of 10 Ω [7]. Since PLA characteristics are often dependent on extrusion parameters [8], [9], initial bulk resistivity measurements are performed at DC on different printed samples. All samples are printed using a Bambu Labs P1S FDM 3D printer with a 0.4mm nozzle and a layer height lh of 0.10mm. The slicer used is Bambu Studio with the preset 0.12mm Fine @BBL X1C (modified layer height to 0.10mm and solid infill). Each sample has a defined set of external dimensions: L indicates the length of the sample, H indicates the height of the sample, W indicates the width of the sample and R indicates the measured resistance in Ω. Equation (3) calculates the resistivity ρ and conductivity σ of the sample material as a function of the previous variables.

$$\rho = \frac{1}{\sigma} = R\cdot\frac{W\cdot H}{L} \quad (3)$$

Samples with a fixed L = 30mm and W = 10mm are fabricated, the remaining parameters and measurement results are shown in Table I.

TABLE I
SAMPLE MEASUREMENTS FOR lh = 0.1mm

H	R	ρ	σ
1	0.302 kΩ	10.1 Ω · cm	9.90 S/m
2	0.162 kΩ	10.8 Ω · cm	9.25 S/m
3	0.115 kΩ	11.5 Ω · cm	8.69 S/m
4	0.088 kΩ	11.7 Ω · cm	8.54 S/m

The average DC ρ is 11.025 Ω · cm, which corresponds with a surface resistivity of 11.025 Ω, similar to that indicated by the manufacturer [7]. The σ initially used to model and simulate the absorber is estimated by using the average ρ previously calculated, being the result 9.09 S/m .

On electromagnetic simulators this material can be simulated as a lossy metal or a dielectric. As the resistivity is high some test samples has been used to measure the behavior with frequency and the best agreements between simulations and measurements have been obtained modeling the material as a dielectric with a σ of 52 S/m, and an ϵ_r of 2.44, corresponding with that of a normal PLA [8], [9].

The material is further characterized by using 2 Wr90 waveguides, connecting them with a 0.2mm thick sheet of the conductive PLA material between them and measuring S21 at 10.25GHz. The measured S21 is -10.5dB while a CST MWS simulation using the previously described properties shows a S21 of -11dB. Fig. 2 shows both setups.

(a) (b)

Fig. 2. (a) Waveguide measurement setup. (b) CST MWO simulation.

D. Synthesis of the absorber

The absorber is modelled parametrically as a unitary cell in CST MWS. Initially defining r_{in}, α, δ, ϵ_r and $\tan\delta$ as constants, the rest of the parameters are modified as iterated upon until consistent patterns are found among the results. Throughout this process the ability to find a way to control the amount of absorption and shift working frequencies is prioritized. The absorber is fabricated, measured and the conductivity model is then modified to follow the observed result. It is observed that by changing the D versus r_{trim} ratio γ_1 described by Equation (4), the absorption response is altered. This way, a lower γ_1 allows for a more pronounced absorption. A γ_1 of 2.16 is found to be optimal to obtain an absorption of over 15 dB while allowing for permissible fabrication tolerances.

$$\gamma_1 = \frac{D}{r_{trim}} \quad (1)$$

It is also observed that by changing D and t_S proportionally, the lowest working frequency f_L is shifted with minimum effect on the absorption and bandwidth 0. A ratio γ_2 of 3.57 defined by Equation $\gamma_2 = \frac{D}{t_S}$ (2) is found to be optimal in terms of bandwidth and ripple for the given σ.

$$\gamma_2 = \frac{D}{t_S} \quad (2)$$

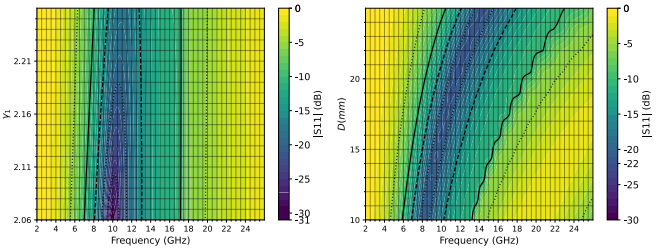

(a) (b)

Fig. 3. (a) Effect on the bandwidth versus absorption ratio of the absorber. (b) Effect on the working frequency of the absorber.

After optimizing the parameters, the considered optimum values for absorption in the X band (8 to 12 GHz) are displayed on Table II and the final 3D model on Fig. 4.

TABLE II
DESIGN PARAMATERS FOR f_L = 8GHZ

D	t_{CT}	t_S	t_{CG}
15mm	0.4mm	4.2mm	0.4mm

r_{in}	r_{trim}	N	α	δ
0.75mm	6.94mm	1	$\frac{\pi}{2}$ rad	$\frac{\pi}{8}$ rad

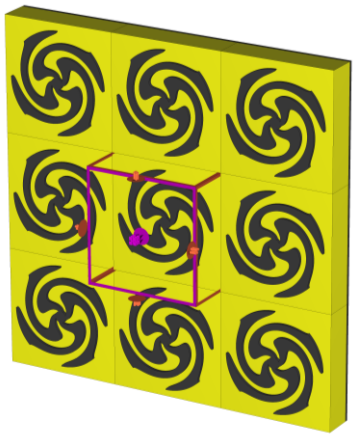

Fig. 4. 3D view of the absorber array.

The absorber is tested for polarization diversity using linear vertical (TE) and horizontal (TM), as well as both circular (RHC y LHC) polarizations, no difference in the reflection coefficient is observed for an orthogonal incident angle. In Fig. 5 it can be clearly observed how the power loss is distributed over the FSS depending on the polarization used. The linear polarizations show a defined vertical or horizonal pattern, whilst the circular polarizations show the highest loss on the turn aligned with their angular direction.

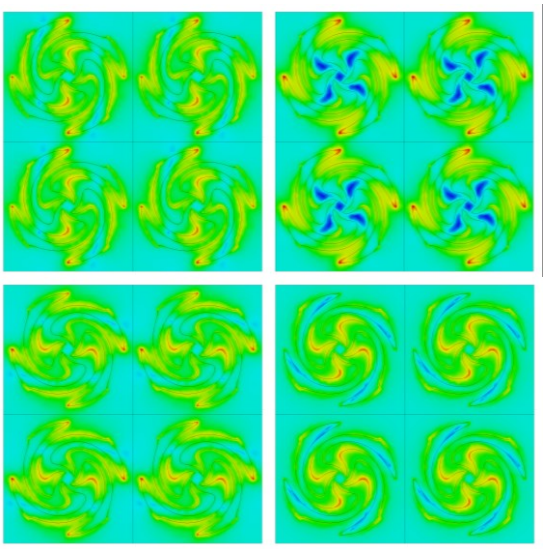

(a) (b)

Fig. 5. Power loss density distribution at 10GHz (a) top TE and bottom TM polarizations and (b) top RHC and bottom LHC polarizations.

The absorber is also characterized by the effects on the absorption response caused by changing the incident wave angle θ Fig. 6. The absorber maintains a relatively stable response up to 40° for a TM polarization, where it can be observed displacing f_L towards higher frequencies, at 50° the response has rapidly degraded over most of the band. For a TE polarization, the response degrades linearly relative to θ.

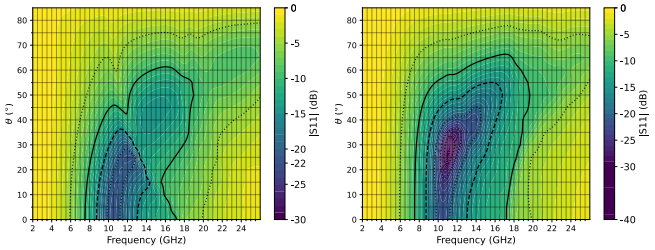

(a) (b)

Fig. 6. Effect on the absorption response by changing the incident angle θ for (a) TE polarization and (b) TM polarization.

III. Measurements of the Absorber

The absorber is measured at a distance of 1m using a vector network analyzer (VNA) connected to 2 wideband EMC horn antennas (1-18GHz) type BHA9118 as pictured in Fig. 7.

S21 measurements are made to enhance the dynamic range of the system. The antennas and cables were calibrated using a metal plane located in the same position of the absorber. One the system is calibrated the metal plane is replaced by the absorber measuring the variation. Measurements were made on a frequency sweep covering 3-18 GHz shown on figure 7. Results show good agreement with simulations although there is a remarkable difference in the higher frequency range. This difference is mainly due to the important dependence of conductivity of graphite loaded PLA with frequency.

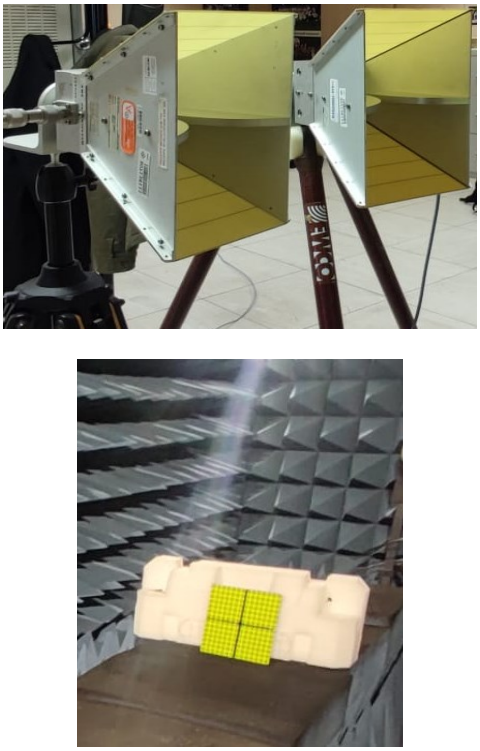

Fig. 7. Pictures of the measurement setup.

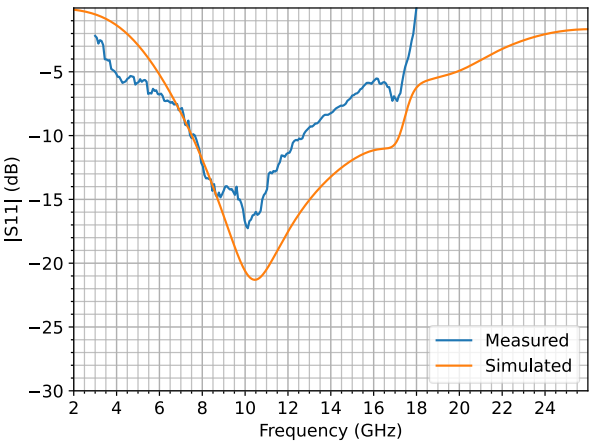

Fig. 8. Absorption response of the fabricated absorber.

IV. Conclusions

In this paper, the proof of concept of designing multilayer FSS absorbers based on 3D printed materials is shown. The fabricated absorber offers 15 dB of absorption within most of the X band (8-12GHz) in a compact format and is made using only 3D printed FDM techniques without the need for any post processing.

The absorption performance of the fabricated absorber shows a good correlation with the simulated results. The discrepancy of the absorption between measurement and simulation is within 5 dB, mainly due to the variation of conductivity of the graphite loaded filament. Also, the filling factor of the base dielectric material has some influence on the dielectric constant and on the frequency resonance.

However, the hole process of modeling with CST, manufacturing 3D printer and measurement has shown good agreement between measurements and simulations, and a careful modeling of the conductivity of the graphite filament and the use of a better performance dielectric materials will provide a wider bandwidth and a better absorption performance.

Acknowledgements

Thanks to all the members of APIDE and AETEL for their support to consistently print with conductive materials.

References

[1] B. A. Munk, "Frequency Selective Surfacxes: Theory and Design," Wiley, New York, 2000.

[2] Ye Han, Yumei Chang, Wenquan Che, "Frequency-Selective Rasorbers," *IEEE Microwave Magazine,* vol. 23, no. 2, pp. 86-98, 2022.

[3] Filippo Costa, Agostino Monorchio, "A Frequency Selective Radome With Wideband Absorbing Properties," *IEEE Transactions on Antennas and Propagation,* vol. 60, no. 6, pp. 2740 - 2747, 2012.

[4] Zhongxiang Shen, Jiang Wang, Bo Li, "3-D Frequency Selective Rasorber: Concept, Analysis, and Design," *IEEE Transactions on Microwave Theory and Techniques,* vol. 64, no. 10, pp. 3087-3096, 2016.

[5] Wei Zhang, Rui Mi, Victor Khilkevich, "3D Printed Multilayer Microwave Absorber," *2022 IEEE International Symposium on Electromagnetic Compatibility and Signal/Power Integrity, EMCSI 2022,* pp. 59-63, 2022.

[6] Wei Jiang, Leilei Yan, Hua Ma, Ya Fan, Jiafu Wang, Mingde Feng, Shaobo Qu, "Electromagnetic wave absorption and compressive behavior of a three-dimensional metamaterial absorber based on 3D printed honeycomb," *Sci Rep,* vol. 8, no. 4817, 2018.

[7] CAPIFIL, "750 g PLA CONDUCTEUR 3D printing filament," CAPIFIL, [Online]. Available: https://www.capifil-extrusion-plastique.fr/en/product/750-g-pla-conducteur-3d-printing-filament/.

[8] A. J. Rodríguez, "Exploración de las posibilidades de la impresión 3D en el diseño de componentes de radiofrecuencia," Universidad Autónoma de Madrid, Madrid, 2018.

[9] C. Dichtl, P. Sippel, S. Krohns, "Dielectric Properties of 3D Printed Polylactic Acid," *Advances in Materials Science and Engineering,* vol. 2017, no. July 2017, pp. 1-10, 2017.

[10] R. H. DuHamel, "Dual polarized sinuous antennas". US Patent US06/703,042, 19 02 1985.

[11] Ibrahim M. Alotaibi, Jiasheng Hong, Sultan K. Almorqi, "Cavity-backed dual linear polarization sinuous antenna with integrated microstrip balun feed," in *2015 IEEE 15th Mediterranean Microwave Symposium (MMS)*, Lecce, 2015.

[12] D. A. Crocker, "Numerical and experimental evaluation of sinuous antennas for remote sensing applications," Georgia Institute of Technology, Atlanta, 2019.